ISSN 0023-1584, Kinetics and Catalysis, 2009, Vol. 50, No. 1, pp. 26–30. © Pleiades Publishing, Ltd., 2009.
Original Russian Text © K.V. Romanenko, O.B. Lapina, V.L. Kuznetsov, J. Fraissard, 2009, published in Kinetika i Kataliz, 2009, Vol. 50, No. 1, pp. 31–35.

FIFTY YEARS
OF THE BORESKOV INSTITUTE OF CATALYSIS

Potential of ^{129}Xe NMR Spectroscopy of Adsorbed Xenon for Testing the Chemical State of the Surface of Mesoporous Carbon Materials Illustrated by the Example of Aggregates of Diamond and Onion-Like Carbon Nanoparticles

K. V. Romanenko[a], O. B. Lapina[a], V. L. Kuznetsov[a], and J. Fraissard[b]

[a] *Boreskov Institute of Catalysis, Siberian Branch, Russian Academy of Sciences, Novosibirsk, 630090 Russia*
[b] *Laboratoire de Physique Quantique, UMR CNRS 7142, Ecole Supérieure de Physique et de Chinie Industrielles (ESPCI), 75231 Paris Cedex 05, France*
e-mail: kostaromavita@ngs.ru

Received February 27, 2008

Abstract—The chemical shift in the ^{129}Xe NMR spectrum of adsorbed xenon is very sensitive to the presence of oxygen-containing functional groups on the surface of mesoporous carbon materials. Well-characterized, structurally similar nanodiamond and onion-like carbon samples are considered here as model objects.

DOI: 10.1134/S0023158409010042

Detailed structural studies of carbon materials and carbon-based catalysts usually require a wide variety of physicochemical methods. Conventional sorption and microscopic methods do not always provide complete and reliable information, making it necessary to take alternative approaches. NMR spectroscopy occupies an important place among the physicochemical methods. The NMR spectroscopy of adsorbed xenon is attractive as an independent method for examination of porous materials and catalysts. With its two magnetic isotopes (^{129}Xe and ^{131}Xe), xenon is an ideal atom for this purpose. Its NMR parameters are very sensitive to its environment, including weak van der Waals interactions. The ^{129}Xe isotope has a nuclear spin of 1/2, and its natural abundance, 26.4%, is sufficient for NMR applications, providing an absolute sensitivity of 5.60×10^{-3}. The basic NMR parameter is the chemical shift. The investigated range of its values extends up to 7500 ppm. Chemical shifts of up to 1500 ppm characterize physical adsorption. Perturbations in the electron shell of xenon change the local magnetic field around the nucleus and shift the resonance frequency. The main approximations of the method have been reported in several reviews [1–3].

For gaseous xenon [4] and for porous materials that do not contain any significant amounts of paramagnetic impurities or high electric charges due to impurity cations, the isotropic chemical shift of ^{129}Xe can be represented as a power series in local density (ρ) with temperature-dependent coefficients [5]:

$$\delta(T, \rho) = \delta_s(T) + \delta_{Xe\text{–}Xe}(T)\rho + \delta_{Xe\text{–}Xe\text{–}Xe}(T)\rho^2 + \ldots. \quad (1)$$

For impurity-free materials, δ_s can be viewed as a fundamental characteristic of the surface depending on the rate of xenon exchange between the surface and the pore space. The term $\delta_{Xe\text{–}Xe}\rho$ accounts for the binary collisions of xenon atoms in the pores and depends on the pore dimensionality and geometry. The terms containing powers of density higher than unity ($\delta_{Xe\text{–}Xe\text{–}Xe}\rho^2$ and on) are significant only at rather high xenon densities of $\rho \geqslant 10$ mmol/cm^3. For comparison, the xenon density under normal conditions is $\rho \sim 0.05$ mmol/cm^3.

Although the ^{129}Xe NMR method proved to be an efficient tool for examination of the pore structure and surfaces of silica-based materials (zeolites, silica gels, porous glasses, etc.), it has relatively rarely been applied to carbon-based systems [6–21].

EXPERIMENTAL

A sample of detonation nanodiamonds (NDs) was isolated from the products of detonation of a trinitrotoluene–hexogen mixture using the technology described in [22] and ozone cleaning [23]. The finest ND fractions were separated by centrifuging polydisperse NDs. A sample of onion-like carbon (OLC) was prepared by vacuum annealing of an ND sample at 1900 K [24]. In order to obtain "onions" with a more defective surface, part of the OLC sample was subjected to oxidative treatment (the resulting sample is designated OLC-ox). Oxidation was carried out in a flowing $O_2 + N_2$ (1 : 50) mixture at 843 K for 2 h.

Carbon samples were characterized by low-temperature (77 K) nitrogen adsorption. The specific surface area was measured by the BET method. The total spe-

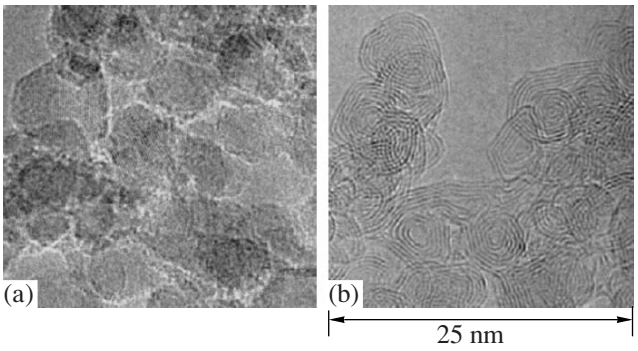

Fig. 1. TEM images of (a) ND and (b) OLC.

cific pore volume (V_t) was derived from adsorption data obtained at a relative pressure of $P/P_s = 0.98$. The mean pore diameter was calculated within the model of intersecting cylindrical pores open on both sides ($D = 4V/S$, where V is the volume and S is the surface area). The pore size distribution was derived from the desorption branches of isotherms using the de Boer–Brockhoff approximation.

Electron micrographs were obtained using a JEM-2010 microscope. OLC powders were deposited onto an amorphous carbon–coated copper grid by ultrasonic spraying of ethanolic suspensions.

Experiments were carried out using isotopically enriched xenon (~99% ^{129}Xe). In some cases, we used an optical xenon spin polarization technique [25] for enhancing the sensitivity of the method. A xenon + helium stream with preset partial pressures, generated by a pump, was circulated through a rubidium vapor cell and a sample tube. Rubidium was evaporated by heating the cell to 433–473 K. The cell outlet was water-cooled for rubidium collection. For exciting electronic sublevels of rubidium, the cell was irradiated with a continuous-wave laser (30 W, $\lambda = 794.7$ nm).

Carbon samples (0.5 g) were conditioned in vacuo (10^{-2} Pa) for 10 h at 523 K in glass tubes ($d = 10$ mm) connected to a coaxial vacuum valve. NMR spectra were recorded on an AMX300 pulsed Fourier-transform spectrometer (Bruker) operating at 83 MHz. The number of accumulations was 100–10000 at a $\pi/2$-pulse duration of 14 μs and an interpulse delay time of 1–10 s. Chemical shifts in the ^{129}Xe NMR spectrum were referenced against low-pressure gaseous ^{129}Xe.

RESULTS AND DISCUSSION

Physicochemical Properties of the Samples

TEM images of the initial ND and the OLC obtained from it are shown in Fig. 1. The average diameter of the primary ND particles is 4–5 nm. The ND particles form very strong porous aggregates with a characteristic size of 10 nm to several micrometers. According to nitrogen adsorption data, the porous structure of the ND aggregates consists largely of mesopores, whose size distribution is plotted in Fig. 2. Micropores can also be present at contact sites of primary nanoparticles. (Note that both coherent and incoherent interparticle boundaries were detected by TEM.) The textural parameters derived from nitrogen adsorption data are listed in the table.

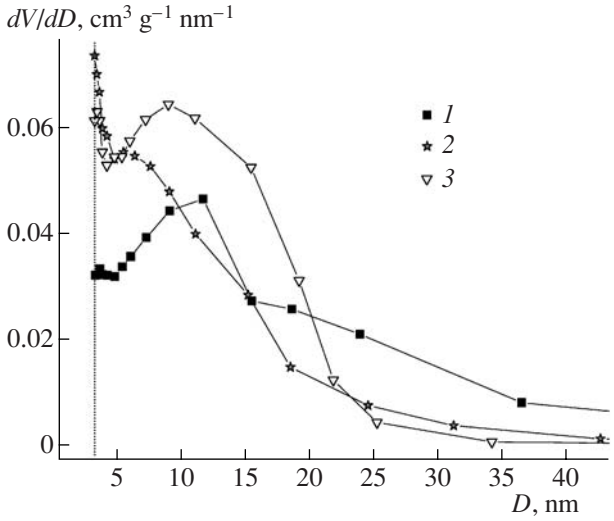

Fig. 2. Pore size distribution for (*1*) ND, (*2*) OLC, and (*3*) OLC-ox.

Chemical analysis data indicate a high concentration of various oxygen- and hydrogen-containing groups on the ND surface (up to 5% of the total sample weight). The sample contains minor amounts (<0.2%) of metals (Fe, Ni, Cr). Since these impurities are irremovable even by severe chemical treatment, they are likely inaccessible to gas molecules.

In the case of OLC, primary nanoparticles also form aggregates by binding together their defective graphite-like layers and by C–C bond formation. The number of fullerene-like layers in an OLC particle varies between 3 and 10. The distance between nearest neighbor layers is 0.35 nm. The OLC surface is graphitized and is structurally similar to the fullerene surface. The porous structure of the OLC aggregates is akin to that of ultrafine nanodiamonds. This is due to the transformation of the primary NDs into OLC particles similar in size.

Textural parameters of ultrafine nanodiamond (ND) and onion-like carbon (OLC and OLC-ox) from N_2 adsorption data

Material	S_{BET}, m^2/g	D, nm	V_t, cm^3/g
ND	288	15.4	1.12
OLC	326	10.4	0.83
OLC-ox	440	9.7	1.04

Note: S_{BET} is the specific surface area, D is the mean pore diameter, and V_t is the total specific pore volume.

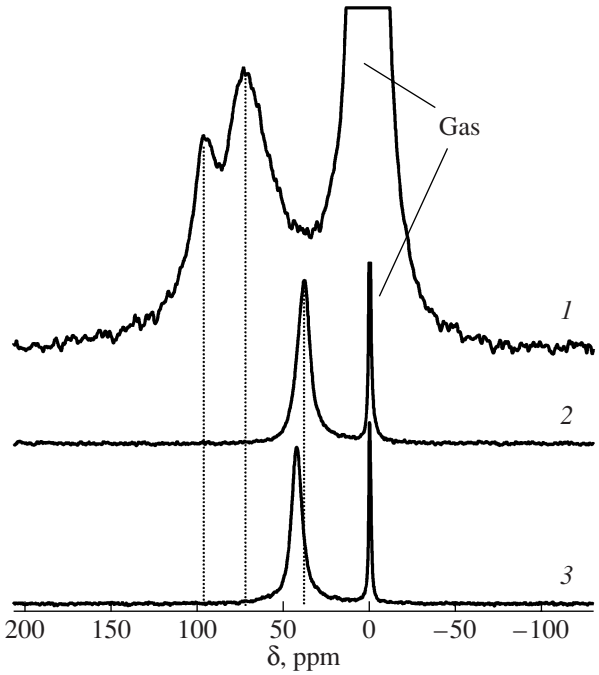

Fig. 3. NMR spectra of optically polarized ^{129}Xe adsorbed on (*1*) ND, (*2*) OLC, and (*3*) OLC-ox.

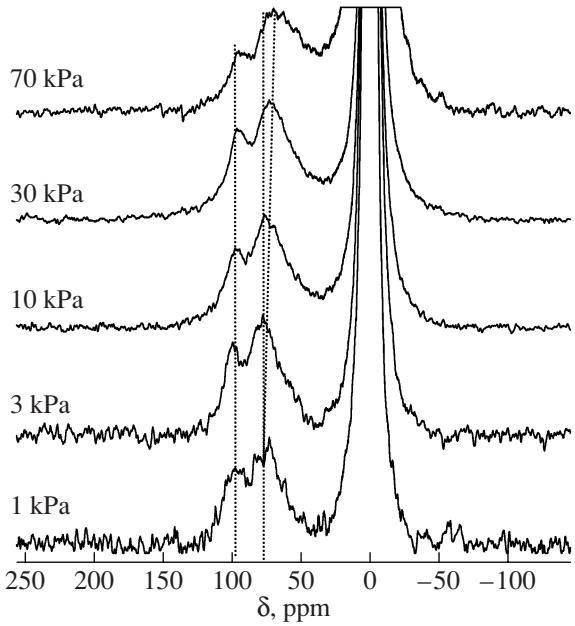

Fig. 4. NMR spectra of optically polarized ^{129}Xe adsorbed on ND at various partial pressures of xenon.

All of the samples have similar ~20-nm-wide pore size distributions without any specific features (see the table). A significant distinction between OLC and ND is that they have different chemical compositions of the surface. According to X-ray spectroscopy data, OLC is a high-purity material based on sp^2-hybrydized carbon. Its purity is due to the fact that all impurities, including metals, are removed at the preparation stage during the high-temperature graphitization of ND in vacuo. Thus, while OLC has a pure graphitized surface with an oxygen content of <0.5% [26], the ND surface is covered with oxygen-containing groups and minor amounts of C–H groups.

^{129}Xe NMR Data

The ^{129}Xe NMR spectrum of optically polarized xenon adsorbed on ND at 298 K is presented in Fig. 3a. The strong line at 0 ppm is due to polarized xenon in the gas phase. The spectrum exhibits two broad components ($\Delta\nu_{1/2}$ ~ 50 ppm) with chemical shifts of 95 and 75 ppm. Under the conditions of this experiment, the intensities of the observed resonances relative to the signal from gaseous xenon do not characterize the real occupancies of adsorption sites. Raising the Xe partial pressure in the 1–70 kPa range does not cause any significant shift of the signals or changes in the line shape (Fig. 4).

Although OLC and OLC-ox have a broad pore size distribution, their ^{129}Xe NMR spectra (Fig. 3, curves *2*, *3*) consist of a single line, which is much narrower ($\Delta\nu_{1/2}$ ~ 10 ppm) than the lines in the spectrum of ND.

The dependences of the ^{129}Xe chemical shifts on the xenon density ρ for OLC and OLC-ox cannot be described by a single linear function (Fig. 5). For the sake of simplicity, they can be divided into two linear portions, namely, A_1 and B_1 for OLC and A_2 and B_2 for OLC-ox (solid lines in Fig. 5). Linear approximation of the two portions led to the following parameters: for OLC,

$\delta_s = 35.7 \pm 0.5$ ppm, $\delta^A_{Xe-Xe} = 82.4 \pm 2$ ppm cm^3 mmol^{-1}, and $\delta^B_{Xe-Xe} = 31.3 \pm 2$ ppm cm^3 mmol^{-1}; for OLC-ox,

$\delta_s = 39.4 \pm 0.5$ ppm, $\delta^A_{Xe-Xe} = 105.7 \pm 5$ ppm cm^3 mmol^{-1}, and $\delta^B_{Xe-Xe} = 31.6 \pm 0.3$ ppm cm^3 mmol^{-1}.

The δ_s values are not large and are typical of graphitized surfaces [11, 12, 14]. Oxidative treatment causes an increase in the chemical shift δ_s because of the increase in the enthalpy of adsorption. From xenon adsorption isotherms measured at different temperatures, the enthalpy of adsorption, ΔH, was estimated at 16.3 kJ/mol for OLC and 24 kJ/mol for OLC-ox. The nonlinear dependence of the chemical shift on the xenon density for OLC and OLC-ox is likely a consequence of the broad pore size distribution. At low xenon densities, adsorption in narrow mesopores is energetically more favorable. At higher xenon densities, the filling of larger mesopores takes place. Thus, the larger slope δ^A_{Xe-Xe}, which corresponds to low xenon densities, refers to narrower mesopores, and δ^B_{Xe-Xe} refers to wider mesopores.

Note that the bulk structure of the nanoparticles forming ND and OLC aggregates, as distinct from the chemical composition of the surface and the pore size of the aggregates, has no effect on the properties of these materials. Since xenon adsorption inside the primary particles is ruled out, the ^{129}Xe NMR data refer only to the surface and the porous structure of ND and OLC, not to their bulk structure.

The large chemical shift and its weak dependence on the xenon density in the case of ND are evidence that there are strong adsorption sites (SAS's) on the surface [1]. The nature of these sites is determined by oxygen-containing groups, and it is the strong interaction of Xe with these groups that is responsible for the large values of the chemical shift (95 and 75 ppm). The broad multicomponent ^{129}Xe NMR signal is further evidence of the existence of SAS's: the strong interaction of xenon with the oxygen-containing groups leads to slow exchange between different surface sites and the gas in the pore space.

In the general case, the ^{129}Xe NMR chemical shift characterizes the interaction between xenon and the surface and can, therefore, be used to study the surface structure and composition. The dependence of the ^{129}Xe NMR chemical shift on the structure of the surface was demonstrated by studies of various types of filamentous carbon [12, 14]. When the surface is chemically and structurally homogeneous, the δ_s value for a given pore size can be viewed as a characteristic of this surface. For ND, the oxygen-to-carbon atomic ratio on the surface is close to 0.5; that is, the concentration of oxygen-containing groups is fairly high. Therefore, the ND surface can be regarded as being uniformly covered with oxygen-containing groups. By contrast, the graphitized surface of OLC is almost free of heteroatoms. Therefore, it can also be viewed as homogeneous. However, when the pore size distribution is wide or rapid exchange takes place, δ_s is not a univocal characteristic of the pore size D. Any observed δ_s is a D-weighted value:

$$\langle \delta_s \rangle = \frac{\int_{D_{min}}^{D_{max}} \delta(D) f(D) \mathrm{d}D}{\int_{D_{min}}^{D_{max}} f(D) \mathrm{d}D}, \quad (2)$$

where D_{min} and D_{max} are the conventional minimum and maximum pore sizes and $f(D)$ is the pore size distribution function.

ND and OLC are a good model system for ^{129}Xe NMR spectroscopy. The pore size distributions (according to nitrogen adsorption data) and textural parameters of OLC and ND are very similar, and this similarity arises from the mechanism of OLC formation from ND. However, the ^{129}Xe NMR parameters (chemical shifts, line widths, and the pressure dependences of the chemical shifts) of these materials are quite different. Taking into account the similarity between the porous structures of ND and OLC, it can be inferred that the radical dissimilarity between the ^{129}Xe NMR data for these materials most likely arises from the difference between the chemical compositions of their surfaces. The chemical shifts (δ_s) observed for OLC and OLC-ox are also different because of the stronger interaction of xenon with the OLC-ox surface.

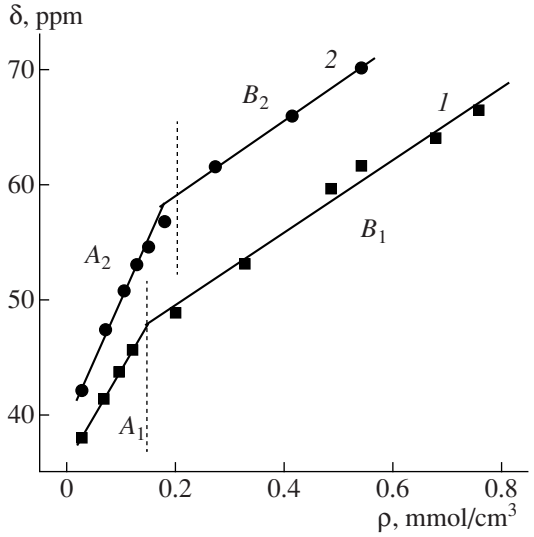

Fig. 5. ^{129}Xe NMR chemical shift as a function of the adsorbed xenon density for (*1*) OLC and (*2*) OLC-ox. The solid lines are linear fits to the portions A_1, S_2, B_1, and B_2 of the spectra.

The ^{129}Xe chemical shift is very sensitive to weak van der Waals interactions. In some cases, this circumstance allows one to obtain valuable information concerning surface defects, the presence of micropores, and the functional groups of the object examined. Because of their structural and chemical heterogeneity, mesoporous carbon materials are rather complicated objects for ^{129}Xe NMR studies. However, this study has demonstrated that chemically modified mesoporous materials and catalysts with similar porous structures are appropriate objects to be tested by this method.

ACKNOWLEDGMENTS

The authors are grateful to A.V. Nosov for technical assistance in experiments involving the optical spin polarization of xenon.

REFERENCES

1. Bonardet, J.L., Fraissard, J., Gedeon, A., and Springuel-Huet, M.A., *Catal. Rev. Sci. Eng.*, 1999, vol. 41, p. 115.
2. Barrie, P.J. and Klinowski, J., *Prog. Nucl. Magn. Reson. Spectrosc.*, 1992, vol. 24, p. 91.
3. Raftery, D. and Chmelka, B.F., in *NMR Basic Principles and Progress*, Berlin: Springer, 1994, vol. 30, p. 112.

4. Jameson, A.K., Jameson, C.J., and Gutowsky, H.S., *J. Chem. Phys.*, 1970, vol. 53, p. 2310.
5. Ito, T. and Fraissard, J., *J. Chem. Phys.*, 1982, vol. 76, p. 5225.
6. Bansal, N., Foley, H.C., Lafyatis, D.S., and Dybowski, C., *Catal. Today,* 1992, vol. 14, p. 305.
7. Tsiao, C.C. and Botto, R.E., *Energy Fuels,* 1991, vol. 5, p. 87.
8. Suh, D.J., Park, T.J., Ihm, S.K., and Ryoo, R.J., *J. Phys. Chem.*, 1991, vol. 95, p. 3767.
9. Wernett, P.C., Larsen, J.W., Yamada, O., and Yue, H.J., *Energy Fuels,* 1990, vol. 4, p. 412.
10. McGrath, K.J., *Carbon,* 1999, vol. 37, p. 1443.
11. Saito, K., Kimura, A., and Fujiwara, H., *Magn. Reson. Imaging*, 2003, vol. 21, p. 401.
12. Simonov, P.A., Filimonova, S.V., Kryukova, G.N., Boehm, H.P., Moroz, E.M., Likholobov, V.A., and Kuretzky, T., *Carbon,* 1999, vol. 37, p. 591.
13. Romanenko, K.V., Py, X., d'Espinose de la Caillerie, J.-B., Lapina, O. B., and Fraissard, J., *J. Phys. Chem. B*, 2006, vol. 110, p. 3055.
14. Romanenko, K.V., d'Espinose de la Caillerie, J.-B., Fraissard, J., Reshetenko, T.V., and Lapina, O.B., *Microporous Mesoporous Mater.*, 2005, vol. 81, p. 41.
15. Romanenko, K.V., Fonseca, A., and Dumonteil, S., Nagy J. B., d'Espinose de la Caillerie, J.-B., Lapina, O.B., and Fraissard, J., *Solid State Nucl. Magn. Reson.*, 2005, vol. 28, p. 135.
16. Romanenko, K.V., Simonov, P.A., Abrosimov, O.G., Lapina, O.B., and Fraissard, J., *React. Kinet. Catal. Lett.*, 2007, vol. 90, no. 2, p. 355.
17. Romanenko, K.V., Lapina, O.B., Espinose, J.-B., and Fraissard, J., *Microporous Mesoporous Mater.*, 2007, vol. 105, p. 118.
18. Clewett, C.F.M. and Pietra, T., *J. Phys. Chem. B*, 2005, vol. 109, p. 17 907.
19. Kneller, J.M., Soto, R.J., Surber, S.E., Colomer, J.-F., Fonseca, A., Nagy, J.B., van Tendeloo, G., and Pietra, T., *J. Am. Chem. Soc.*, 2000, vol. 122, p. 10591.
20. Ago, H., Tanaka, K., Yamabe, T., Miyoshi, T., Takegoshi, K., Terao, T., Yata, S., Hato, Y., Nagura, S., and Ando, N., *Carbon,* 1997, vol. 35, p. 1781.
21. Raftery, D., Long, H., Meersmann, T., Grandinetti, P.J., Reven, L., and Pines, A., *Phys. Rev. Lett.*, 1991, vol. 66, p. 584.
22. Lyamkin, A.I., Petrov, E.A., Ershov, A.P., Sakovich, G.V., Staver, A.M., and Titov, V.M., *Dokl. Akad. Nauk SSSR*, 1988, vol. 302, p. 611.
23. RF Patent 2077476, 1997.
24. Kuznetsov, V.L., Chuvilin, A.L., Butenko, Yu.V., Mal'kov, I.Yu., and Titov, V.M., *Chem. Phys. Lett.*, 1994, vol. 222, p. 343.
25. Anthony, L.Z., Bhavin, B.A., and Clifford, R.B., *J. Magn. Reson.*, 2002, vol. 159, p. 175.
26. Butenko, Yu.V., Krishnamurthy, S., Chakraborty, A.K., Kuznetsov, V.L., Dhanak, V.R., Hunt, M.R.C., and Siller, L., *Phys. Rev. B: Condens. Matter*, 2005, vol. 71, p. 075420.